Diagnosing atmospheric motion vector observation errors for an operational high resolution data assimilation system

Article

Published Version

It is advisable to refer to the publisher's version if you intend to cite from the work. See Guidance on citing.

RMetS

Royal Meteorological Society

Diagnosing atmospheric motion vector observation errors for an operational high-resolution data assimilation system

M. Cordoba,[a] S. L. Dance,[a]* G. A. Kelly,[b] N. K. Nichols[a] and J. A. Waller[a]

[a]*School of Mathematical and Physical Sciences, University of Reading, UK*
[b]*MetOffice@Reading, University of Reading, UK*

*Correspondence to: S. Dance, Meteorology Department, University of Reading, Earley Gate, Berkshire, RG6 6BB, UK.
E-mail: s.l.dance@reading.ac.uk*

This article is published with the permission of the Controller of HMSO and the Queen's Printer for Scotland.

Atmospheric motion vectors (AMVs) are wind observations derived by tracking cloud or water-vapour features in consecutive satellite images. These observations are incorporated into numerical weather prediction (NWP) through data assimilation. In the assimilation algorithm, the weighting given to an observation is determined by the uncertainty associated with its measurement and representation. Previous studies assessing AMV uncertainty have used direct comparisons between AMVs with collocated radiosonde data and AMVs derived from Observing System Simulation Experiments (OSSEs). These have shown that AMV error is horizontally correlated with the characteristic length-scale up to 200 km. In this work, we take an alternative approach and estimate AMV error variance and horizontal error correlation using background and analysis residuals obtained from the Met Office limited-area, 3 km horizontal grid-length data assimilation system. The results show that the observation-error variance profile ranges from $5.2 - 14.1 \, \text{s} \, \text{m}^2 \, \text{s}^{-2}$, with the highest values occurring at high and medium heights. This is indicative that the maximum error variance occurs where wind speed and shear, in combination, are largest. With the exception of AMVs derived from the High Resolution Visible channel, the results show horizontal observation-error correlations at all heights in the atmosphere, with correlation length-scales ranging between 140 and 200 km. These horizontal length-scales are significantly larger than current AMV observation-thinning distances used in the Met Office high-resolution assimilation.

Key Words: AMVs; data assimilation; correlated observation error; SEVIRI; UKV

Received 23 May 2016; Revised 2 September 2016; Accepted 13 September 2016; Published online in Wiley Online Library

1. Introduction

Atmospheric motion vectors (AMVs) are wind observations derived from satellite images by identifying a feature and later tracking it in consecutive images. Suitable features for tracking include clouds or gradients in water vapour (Nieman *et al.*, 1993). The first AMV derivation algorithms were developed in the second half of the 1970s and AMVs have been used in numerical weather prediction (NWP) since the 1990s (Schmetz *et al.*, 1993). The assimilation of AMVs has a positive impact on predictability of operational forecast systems (Cardinali, 2009; Joo *et al.*, 2012).

The AMV derivation process is composed of three main steps: suitable feature selection, wind-vector calculation by measuring the displacement of the tracked feature in consecutive images and height assignment by converting the brightness temperature to pressure. (The derivation also includes an initial preprocessing step and quality-control procedures at the end.) Currently,

wind-speed observations are derived from medium-size features without rapid mutation and exclusively horizontal displacement, meaning that AMVs can describe the general atmospheric flow only. With the introduction of satellites with rapid scan modes, it is becoming possible to capture convective-scale features, although currently this information is not used routinely by all NWP centres. The derivation process has the potential to introduce errors into the observations. The two main sources are tracking and height-assignment error (Forsythe and Doutriaux-Boucher, 2005; Cotton and Forsythe, 2010). These and other sources of error are discussed in more detail in section 3.2.

AMVs are incorporated into NWP through data assimilation. Data assimilation provides techniques for combining observations of atmospheric variables with a priori knowledge of the atmosphere to obtain a consistent representation known as the analysis. Each contribution is weighted by an inverse error covariance matrix; hence it is crucial to the accuracy of the

Reference	Scenario	Error variance	Error correlation
Bormann et al. (2003)	Co-located radiosonde	2.7–3.5	150–210
Bedka et al. (2008)	Co-located radiosonde	1.5–5.0	—
Hernandez-C. and Bormann (2009)	OSSE (10 km grid)	2.5–7.5	120–140
Bormann et al. (2014)	OSSE (2 km grid)	5.5–7.0	120–140

analysis that these error statistics be specified correctly. Quantifying observation-error correlations is not a straightforward problem, because they can only be estimated in a statistical sense, not observed directly. AMVs are continuously monitored by the Satellite Application Facility for Numerical Weather Prediction (NWP-SAF).* This group has produced documents in which the sources of error are described in detail (Forsythe and Doutriaux-Boucher, 2005; Cotton and Forsythe, 2010) and the two main error sources, tracking and height-assignment error, have been assessed individually. It has been shown that, when the height-assignment error is small, the tracking error, estimated using *observation-minus-background* statistics, from the ECMWF and Met Office systems ranges from 2–3 m s^{-1} (Lean *et al.*, 2015). The height-assignment error has been estimated by Folger and Weissmann (2014), Hernandez-Carrascal and Bormann (2014), Lean *et al.* (2015) and Salonen *et al.* (2015) using the technique of *best-fit statistics*. The errors have been quantified within a range of 50–150 hPa. Overall, the error in the height assignment accounts for the larger AMV uncertainty, contributing to 70% of the total error (Velden and Bedka, 2009).

Previous studies estimating AMV observation-error statistics carried out direct comparisons between AMVs with collocated radiosonde data (Hollingsworth and Lönnberg, 1986; Bormann *et al.*, 2003; Bedka *et al.*, 2008) or AMVs derived from Observing System Simulation Experiments (OSSEs: Bormann *et al.*, 2010b, 2014; Lean *et al.*, 2015). The main results of these studies (summarized in Table 1) show that AMV error variances range from 1.5–7.5 m s^{-1} and that AMV error is correlated with length-scales between 120 and 210 km. This correlation is likely to arise as, by their nature, AMVs are not randomly distributed in space or time and hence similar errors can afflict a region of AMVs. The results also show a relatively small difference in both error variance and error correlation between infrared and water-vapour channels. However, both these approaches have limitations; the OSSE studies use simulated rather than real observations and the collocated radiosonde studies suffer from lack of available data.

The new contribution of the work presented in this article is the estimation of AMV error statistics for the Met Office limited-area high-resolution data assimilation system, using the diagnostic of Desroziers *et al.* (2005). To the best of our knowledge, this type of study has not previously been undertaken with AMV observations. The diagnostic uses a combination of observation-minus-background innovations and observation-minus-analysis residuals. By calculating the expectation of the outer product of these residuals over a large number of analysis cycles, the observation-error structure can be estimated. Desroziers *et al.* (2005, 2009) and Ménard *et al.* (2009) used the diagnostic in toy models with predefined *true* observation and background errors and found that iterative runs of the diagnostics converge to the exact value of the observation-error covariance matrix. Further theoretical and idealized results relating to the diagnostic under some simplifying assumptions provide information on how to interpret the results of iterating the diagnostic when the errors used in the assimilation are not exact (Chapnik *et al.*, 2004, 2006; Ménard, 2016). However, in operational data assimilation systems, successive iterations are too costly in terms of computation

and the software does not exist to include spatially correlated errors. In the case where only one iteration is possible, the theoretical work of Waller *et al.* (2016b) can provide insight on how to interpret the results of the diagnostic. Despite the limitations of the diagnostic, it has been used successfully in simple model experiments in both variational (Stewart, 2010) and ensemble (Li *et al.*, 2009; Miyoshi *et al.*, 2013) data assimilation systems and to estimate time-varying observation errors (Waller *et al.*, 2014a). The diagnostic has also been applied to operational NWP and to calculate satellite inter-channel error covariances (Stewart *et al.*, 2009, 2014; Bormann and Bauer, 2010; Bormann *et al.*, 2010a, 2016; Weston *et al.*, 2014; Waller *et al.*, 2016a) and spatial error covariances (Waller *et al.*, 2016a,c) in variational assimilation systems, as well as in ensemble data assimilation systems (Schraff *et al.*, 2016; Lange and Janjić, 2015). Inter-channel observation-error covariance matrices calculated using the diagnostic have been implemented in variational assimilation systems and have improved forecast skill (Weston *et al.*, 2014; Bormann *et al.*, 2016).

In this article, the Desroziers *et al.* (2005) diagnostic theory and its numerical implementation are described in section 2. An introduction to AMV observations is given in section 3. We describe their derivation, limitations and known sources of error. The experimental scenario, including details of the operational Met Office high-resolution data assimilation system and AMVs used in this study, is found in section 4. Our results are shown in section 5. These show that the observation-error variances vary with height, with the largest error variances occurring at the mid and high levels, where the influence of wind speed and shear is largest. The estimated variances are larger than those derived in previous studies, but lower than the variance used in the operational assimilation system. The horizontal error correlation length-scales for AMVs at all pressure levels range between 150 and 210 km. These length-scales are similar to results found in previous studies and are likely to be a result of height assignment and tracking errors. We conclude in section 6, where we discuss our results in the context of the previous literature and note that the observation-error correlation lengths are much longer than the observation thinning length-scales currently used in the Met Office high-resolution assimilation.

2. Desroziers *et al.* (2005) diagnostic

Recently, the Desroziers *et al.* (2005) method has been applied to estimate the observation and background-error structure in current data assimilation systems. The main theoretical aspects of the diagnostic and its numerical implementation for this work are introduced in this section.

2.1. Theoretical description

The Desroziers *et al.* (2005) diagnostic for the observation-error covariance matrix makes use of *Observation-minus-background* and *Observation-minus-analysis* residuals available following completion of the assimilation process. The *Observation-minus-Background* residual (or innovation) in its linear form is

$$\mathbf{d}_\mathrm{b}^\mathrm{o} = \mathbf{y} - \mathbf{H}\mathbf{x}^\mathrm{b}, \qquad (1)$$

where $\mathbf{y} \in \mathbb{R}^p$ are the observations, $\mathbf{x}^\mathrm{b} \in \mathbb{R}^n$ is a prior background state and $\mathbf{H} : \mathbb{R}^n \mapsto \mathbb{R}^p$ is a linear observation operator. In this work, the observation operator is simply the linear interpolation of horizontal winds on a model grid to the location of the AMV observation. The *observation-minus-analysis* residual, also in its linear form, is

$$\mathbf{d}_\mathrm{a}^\mathrm{o} = \mathbf{y} - \mathbf{H}\mathbf{x}^\mathrm{a}, \qquad (2)$$

where $\mathbf{x}^\mathrm{a} \in \mathbb{R}^n$ is the analysis. Desroziers *et al.* (2005) showed that the expectation of the outer product is

$$\left\langle \mathbf{d}_\mathrm{a}^\mathrm{o} \mathbf{d}_\mathrm{b}^\mathrm{oT} \right\rangle \approx \mathbf{R}_\mathrm{e}, \qquad (3)$$

where $\mathbf{R_e} \in \mathbb{R}^p$ is an estimate of the observation-error covariance matrix. The diagnostic provides an exact estimate of the observation-error covariance matrix if the specified observation and background-error covariance matrices used in the data assimilation cycle are correct. However, in operational data assimilation systems the *true* specification is not feasible and hence, as pointed out by Todling (2015), careful thought must be applied in interpretation of the results from the diagnostic.

2.2. Diagnostic implementation

The Desroziers *et al.* (2005) diagnostic makes use of the background and analysis residuals to estimate the observation-error covariance matrix $\mathbf{R_e}$ (Eq. (3)) in a multidimensional system. However, within the scope of this work, the AMV observations are of the two wind-speed vector components U and V, the zonal and meridional wind respectively. We treat these as separate scalar observations, or in some cases combine them and consider the wind speed,

$$S = \sqrt{U^2 + V^2}. \qquad (4)$$

Since the observations are derived from cloud tracking, the observations are not available on a fixed grid and the number of observations available at assimilation time varies. In order to make computations tractable, we only compute horizontal observation-error covariances. We define discrete vertical layers of 50 hPa depth and we assume that the error statistics are homogeneous within each of these vertical levels. Furthermore, pairs of observations are binned according to their horizontal separation distance, so that the horizontal correlation function calculated is based on a discretized separation distance. Details of the bin widths etc. are given in section 4.3.

Our numerical implementation of the diagnostic is a scalar version of Stewart (2010, section 4.2.2). Suppose that there are N pairs of observations for the separation distance bin at distance d and vertical level z. If the kth pair of observations in the bin has indices (i_k, j_k), then the covariance is found from Eq. (3) as

$$\mathrm{cov}(z, d) = \frac{1}{N} \sum_{k=1}^{N} (\mathbf{d_a^o})_{i_k} (\mathbf{d_b^o})_{j_k}$$
$$- \left[\frac{1}{N} \sum_{k=1}^{N} (\mathbf{d_a^o})_{i_k} \right] \left[\frac{1}{N} \sum_{k=1}^{N} (\mathbf{d_b^o})_{j_k} \right]. \qquad (5)$$

The second term ensures that the calculation is not affected by bias (Waller *et al.*, 2016a). The error variance, var(z), is calculated using a similar equation, but with $d = 0$ and $j_k = i_k$ for each k. The horizontal error correlation function at a given vertical level z is given by normalizing the observation-error covariance in each separation distance bin by the overall observation-error variance for the horizontal z-plane:

$$\rho(z, d) = \frac{\mathrm{cov}(z, d)}{\mathrm{var}(z)}. \qquad (6)$$

3. Atmospheric motion vectors

3.1. Derivation

AMVs are wind observations derived by tracking water-vapour or cloud features over consecutive satellite images. The AMV derivation process consists of five steps, including pre-processing and post-processing (quality control) (García-Pereda *et al.*, 2012). During the pre-processing step, information is extracted from the NWP model and the satellite sensors, including latitude, longitude, solar and satellite zenith angle matrices, reflectances for any visible channel to be used, brightness temperatures for any infrared or water-vapour channel to be used, NWP

temperature and wind guess. The derivation continues with an initial identification step, in which a suitable feature is selected. The feature must be bright, isolated and with defined edges. Later this feature is tracked in successive images and a displacement vector, the AMV, is calculated. The next step is the height assignment of the feature. This is accomplished using the observed brightness temperature and the NWP background profile. Further details of the height assignment are given in García-Pereda *et al.* (2012). Finally, a quality-control step assigns a Quality Index (QI), based on statistical properties (Holmlund, 1998). During the quality control, an orographic flag is assigned to detect AMVs which, under the influence of land, do not correspond with the general atmospheric flow. The orographic flag is used in NWP to reject AMVs prior to their assimilation.

The derivation of AMVs is a complex process with some inherent assumptions and limitations. AMVs are limited by the satellite sensor characteristics. The feature will not be described with full accuracy when it is larger than a given tracking area or when it mutates faster than a given time interval between consecutive images. The AMV derivation is also limited by the brightness-temperature model used to resolve complex vertical cloud structures, so that AMVs are in essence wind observations made upon thin clouds and those with a single identified cloud type, moving at a constant pressure level. Finally, AMVs are limited to follow the large-scale atmospheric flow, since the QI penalizes observations that are not temporally or spatially homogeneous. These limitations often mean that an AMV cannot be derived or that the observation is removed by the quality control. However, where our understanding of these limitations is poor, these observations may pass the quality control and be used for assimilation. In this case, the limitations mentioned become sources of errors for the AMVs. These and other error sources are described in the next section.

3.2. Sources of error

In data assimilation, the main sources of error associated with observations can be categorized as *pre-processing*, *measurement*, *observation operator* and *representativeness* error. A discussion on these types of error can be found in Daley (1993), Waller *et al.* (2014b) and Lean *et al.* (2015). It is likely that the two main contributors to the total AMV error are as follows.

- **Tracking error**. Tracking the wrong feature during the recognition of consecutive images leads to an error in the displacement vector.
- **Height assignment error**. Errors in the model brightness temperature derivation and in the brightness temperature to pressure conversion lead to an error in the feature's height.

A more detailed discussion of the origin of these errors can be found in Forsythe and Doutriaux-Boucher (2005), Cotton and Forsythe (2010) and Lean *et al.* (2015).

The magnitude of the error is influenced by specific atmospheric situations. All situations that could potentially lead to wind-speed error are not exhaustively described here. We do, however, describe those that are expected to have the largest impact.

- **Mid-level features**. These features have the largest potential to be contaminated by features above or below. This contamination makes mid-level features harder to track and impacts on their brightness-temperature estimate. This in turn may impact on the accuracy of height assigned to the feature.
- **Wind shear**. The wind shear is the rate of the change of wind speed in the vertical. Where the wind shear is low, a height-assignment error will make very little difference to the comparison of AMV and true wind. Where wind shear

is high, a small error in height assignment can introduce a large wind-speed error (see e.g. Salonen *et al.*, 2015, figure 1).

- **Polar Front Jet Stream**. The Polar Front Jet Stream is a well-known meteorological feature, which is a meridional meandering core of high wind speed ($>30 \, \mathrm{m \, s^{-1}}$) at midlatitude, located at about $250-300 \, \mathrm{hPa}$. Its effects can be significant at $\pm5°$ away from its core (Mahlman, 1973). Due to the presence of the Polar Front Jet Stream, the wind profile just below tends to be very steep, consequently yielding a high wind shear. The meridional nature of the Polar Front Jet Stream and the fact that its effects can be significant at $\pm5°$ away from its core means that potentially large areas, $10°$ wide, can be under the influence of a homogeneous high zonal wind speed and, in contrast, a heterogeneous meridional wind speed, leading to larger errors in the meridional AMV observations.

- **Temperature inversion**. When the temperature inversion is sufficiently large and intense, the radiative transfer cannot solve accurately for the radiance at the top of the atmosphere (Leblanc and Hauchecorne, 1997), leading to an inaccurate brightness-temperature estimate.

4. Experiment scenario

4.1. The Met Office UKV model and assimilated AMVs

The NWP model is the Met Office high-resolution convection-permitting model (UKV) over the UK. The interior of the domain has a resolution of 1.5 km. At the edges, the resolution increases smoothly to 4 km. This allows the boundary conditions to spin up before reaching the fixed interior grid. Data is assimilated in 3 h windows using a three-dimensional variational first guess at appropriate time (3D-Var FGAT) assimilation scheme (Lorenc *et al.*, 2000; Lorenc and Rawlins, 2005; Rawlins *et al.*, 2007; Ballard *et al.*, 2016). To calculate estimates of the observation-error covariances, we require the model background fields. The background fields used in this study are the archived background data produced by the operational Met Office system from June, July and August 2013 (JJA2013). To generate the analyses, we run the Met Office high-resolution NWP and data assimilation system under the January 2014 operational configuration.

The AMVs under analysis within this article are derived by applying the High Resolution Wind (HRW) algorithm from the Nowcasting and Very Short Range Forecasting SAF group (NWC-SAF)[†] to data observed using the Spinning Enhanced Visible and Infrared Imager (SEVIRI) on board the *Meteosat-10* MSG satellite. The *Meteosat-10* MSG satellite operates in a geostationary orbit, 36 000 km above the Equator, and returns imagery every 15 min (in full scan mode) and every 5 min in Rapid Scan (covering Europe only: Schmetz *et al.*, 2002). The SEVIRI instrument on board provides image data in 12 different spectral channels, three visible (HRVis, VIS06, VIS08) during daytime only, one near-infrared (NIR), two water vapour (WV062, WV073) and six infrared (IR038, IR087, IR097, IR108, IR120, IR134). The imaging spatial resolution is 3 km at the subsatellite point for standard channels and down to 1 km for the high-resolution visible (HRVis) channel (Schmid, 2000). However, not all the SEVIRI channels are relevant for the derivation of AMVs. The NWC-SAF HRW algorithm has been adapted to derive AMVs from seven different channels and, within these, this work focuses only on the four channels (WV062, WV073, IR108 and HRVis) currently assimilated by the Met Office UKV assimilation system (Ballard *et al.*, 2016). Detailed information about the operational parameters used in the HRW algorithm can be found in García-Pereda *et al.* (2012). The derivation of the AMV results in an observation that is a vertical average over a given volume; however,

Table 2. Selected SEVIRI channels from those assimilated in the 3D-Var FGAT for the initial conditions of the Met Office UKV model.

High level	$100-400 \, \mathrm{hPa}$	IR108	WV062	WV073
Medium level	$400-700 \, \mathrm{hPa}$	IR108		
Low level	$700-1000 \, \mathrm{hPa}$	IR108	HRVis	

in practice the observations are treated as point observations. The AMVs are classified according to vertical level, as recommended by the Working Group on Verification Statistics in the Third International Winds Workshop (Menzel, 1996). Table 2 shows the four SEVIRI channels, along with their height classification, used in the AMV derivation.

Not all the derived AMV observations are assimilated. The quality control rejects observations below a quality index threshold and/or belonging to a blacklist; further details can be found in (García-Pereda *et al.*, 2012). A second source of rejection of derived AMVs is thinning. Thinning is used in NWP to alleviate problems with spatially and temporally correlated observation errors by reducing data density (Forsythe and Saunders, 2008). Over each assimilation window, a predetermined minimum horizontal and vertical separation distance between observations is employed. In consequence, AMV observations that are very close together are rejected.

The Met Office UKV model AMVs selection parameters are as follows:

1. quality-index threshold: QI > 80% (with forecast check);
2. horizontal thinning distance: 20 km; and
3. vertical thinning distance: 100 hPa.

Although the AMV thinning distance within the operational assimilation cycle is 20 km, this work makes use of AMVs within a shorter distance, 5 km, in order to increase the number of observations for robustness in the residual statistics. The number of single observations at all levels and for all channels exceeds 5000 (Figure 1), which is considered robust enough for sample statistics. For the horizontal correlation statistics, the number of observation pairs at all levels and for all channels exceeds 10 000, reaching 700 000 at high level for the WV073 channel.

4.2. Assigned observation-error variance

In order to assimilate AMV observations within the Met Office UKV model 3D-Var FGAT system, each AMV observation has an assigned uncertainty associated. This assigned error is a sum of two parts, each linked to a known physical source of error (as
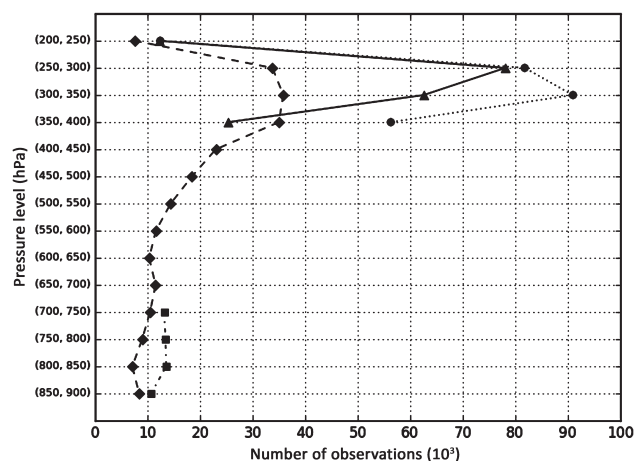

Figure 1. Pressure levels and number of observations (in thousands) for the four SEVIRI channels: IR108 (dashed with diamonds), WV062 (solid with triangles), WV073 (dotted with circles) and HRVis (dash–dotted with squares). Pressure was discretized in 50 hPa intervals, from 200–900 hPa.

described in section 3.2). The two errors that contribute to the assigned error are as follows.

- **Assigned tracking error variance**. $\sigma^2_{\text{tracking}}$ is based on the QI generated during quality control. The assigned error variance (standard deviation) ranges from $6.25 \, \text{m}^2 \, \text{s}^{-2}$ ($2.5 \, \text{m} \, \text{s}^{-1}$) at $QI = 100$ to $20.25 \, \text{m}^2 \, \text{s}^{-2}$ ($4.5 \, \text{m} \, \text{s}^{-1}$) at $QI = 60$.
- **Assigned height error variance**. σ^2_{height} is based on the AMV height error and on the background vertical wind shear. Its derivation is dependent on the satellite, channel, pressure level, surface type, height-assignment method and latitude band. The values are found by analyzing the height-assignment error under different conditions for several months of data. For example, AMVs located at 200 hPa using the CO_2 slicing height assignment are assigned a height error of 40 hPa (Forsythe and Saunders, 2008).

The combination of the assigned tracking error variance and the assigned height error variance gives the total assigned wind-speed error variance $\sigma^2_{\text{assigned}}$ for each of the U and V vector components:

$$\sigma^2_{\text{assigned}} = \sigma^2_{\text{tracking}} + \sigma^2_{\text{height}}. \tag{7}$$

4.3. Experimental assumptions

Some pragmatic assumptions are made in order to process the operational dataset using the Desroziers *et al.* (2005) diagnostic.

4.3.1. Observation separation distance bins

Using the diagnostic, the horizontal correlation function is calculated based on a discretized separation distance. This work uses a 20 km width discretization, e.g. observation pairs with separation distances between 80 and 100 km are put in the same distance bin. In order to separate the horizontal error correlation and to avoid vertical correlation noise, the vertical dimension is discretized too. This work has used 50 hPa height discretization, e.g. observations within 400−450 hPa are considered to be taken at the same pressure level and therefore on the same horizontal plane. The horizontal correlation function calculation assumes that each member of an observation pair has the same validity time. For the purposes of our experiments, only pairs of simultaneous observations are considered. The horizontal, vertical and temporal discretization parameters are in line with Bormann *et al.* (2010b, 2014).

4.3.2. Length-scale

The length-scale L serves as a quantity to indicate the scale of the correlation function, meaning that, beyond L, the correlation is considered insignificant. Within the scope of this report, L is taken to be the value when the estimated correlation falls below a threshold figure of 0.2 (Liu and Rabier, 2002).

5. Results

This section presents the estimated AMV error statistics calculated using the Desroziers *et al.* (2005) diagnostic. The AMV observation-error variance profile has been estimated (section 5.1) and compared with the assigned error variance (section 5.2). Finally, section 5.3 presents the results of the AMV horizontal error correlation estimation.

5.1. Observation-error variance estimate profile

In order to obtain an overview of the changes in diagnosed variance with height, the wind-speed error variance for each
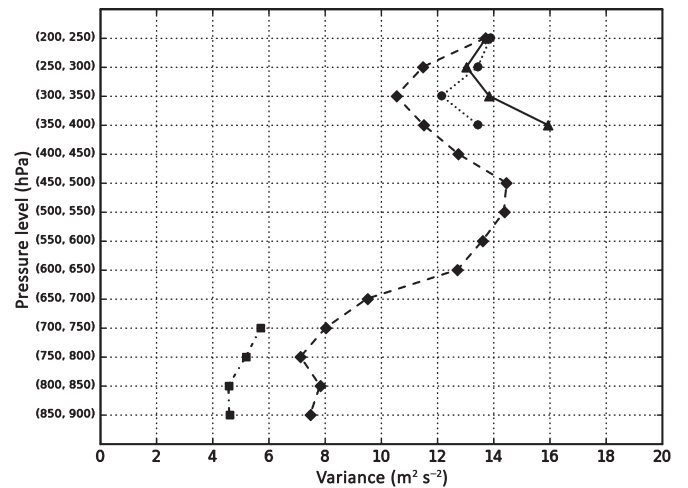

Figure 2. Profile of the AMV wind-speed observation-error variance estimate [$\text{m}^2 \, \text{s}^{-2}$] for four SEVIRI channels: IR108 (dashed with diamonds), WV062 (solid with triangles), WV073 (dotted with circles) and HRVis (dash−dotted with squares). Observations were binned in 50 hPa intervals, from 200−900 hPa.

pressure level bin was calculated for each of the four SEVIRI channels, IR108, WV062, WV073 and HRVis. Figure 2 shows that the AMV observation-error variance estimate profile varies significantly with height, for all channels. The IR08 channel is the only channel with AMV observations across the whole pressure range considered. The other channels follow a similar pattern at levels where these observations are available, although there are quantitative differences between channels.

The error variances diagnosed for the IR08 channel have their maximum value, $14.5 \, \text{m}^2 \, \text{s}^{-2}$, at mid levels between 450 and 550 hPa. This could be caused by two factors acting in combination. Firstly, as discussed in section 3, the processing of mid-level features has a large potential to be contaminated by other features above or below and thus is more likely to suffer from large height-assignment errors. Secondly, regions of high wind shear are expected to result in large AMV error variance. The average wind speed profile is plotted in Figure 3. This has been calculated using all the AMV U and V observations available during the experiment period (JJA 2013). Within the period of analysis, the wind shear is significantly higher in the 500−700 hPa range. As discussed in section 3.2, a height-assignment error in combination with a high wind shear would have a significant impact on the wind-speed error.

Returning to Figure 2, another important feature seen is the relatively high observation-error variance found at high levels
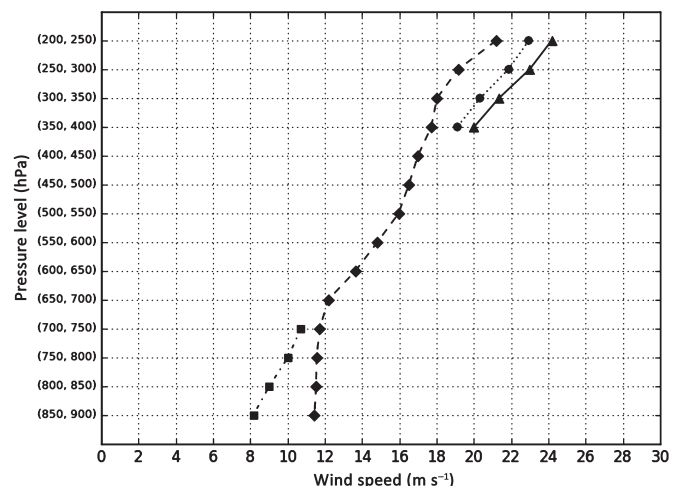

Figure 3. Profile of the average AMV wind speed for four SEVIRI channels: IR108 (dashed with diamonds), WV062 (solid with triangles), WV073 (dotted with circles) and HRVis (dash−dotted with squares). Pressure was discretized in 50 hPa intervals, from 200−900 hPa.

Table 3. AMV wind speed (S), AMV zonal wind speed (U) and AMV meridional wind speed (V) observation-error variance estimate $[m^2 \, s^{-2}]$, for four SEVIRI channels, IR108, WV062, WV073 and HRVis, at high, medium and low levels.

	High level			Medium level			Low level		
	U	V	S	U	V	S	U	V	S
IR108	09.24	10.54	11.42	11.83	11.40	13.08	7.30	8.52	07.72
WV062	11.80	13.05	14.14	–	–	–	–	–	–
WV073	11.06	12.32	13.27	–	–	–	–	–	–
HRVis	–	–	–	–	–	–	5.47	5.23	5.15

(200−250 hPa) for the three SEVIRI channels, IR108, WV062 and WV073. This may be due to the very large assigned variances affecting the results of the diagnostic (see section 5.2). An alternative plausible physically motivated explanation relates to high wind shear at these levels. Due to the presence of the Polar Front Jet Stream, the wind profile just below tends to be very steep. Small errors in combination with high wind shear at a high wind-speed range ($>30 \, m \, s^{-1}$) could potentially have a significant impact on the wind-speed error (section 3). High mean wind shear and a high mean wind speed at the top level (200−250 hPa) are seen in the average wind-speed profile in Figure 3. It is also possible that poor cloud classification could result in significant height-assignment errors at these levels.

An AMV observation consists of the two wind-speed components, U and V. Table 3 summarizes the average observation-error variance estimate for the wind components and speed (U, V and S) for the four SEVIRI channels. Results are divided into high, medium and low levels, as in the Table 2 classification. The comparison of the error variance estimate between channels and between wind-speed vector components shows only relatively small differences. The exceptions are the the HRVis channel and the high-level U and V components. For the high level U and V components, the meridional nature of the Polar Front Jet Stream is likely to be having an impact. The HRVis channel produces AMV observations during daytime only. Near the surface, where the HRVis observations are available, the wind pattern tends to be different at night than during daytime. This may contribute to the significant difference compared with the IR108 channel, which produces AMV observations during day and night.

In general, the AMV error variance estimates $[5.2−14.1] \, m^2 \, s^{-2}$, are a little larger than some of the error variances derived in previous studies, $[1.5−7.5] \, m^2 \, s^{-2}$ (Table 1). However, the methodologies of previous studies were different, being comparisons against either radiosondes or NWP model winds, typically with longer NWP model grid lengths than those considered here. In addition, the behaviour of the Desroziers *et al.* (2005) diagnostic depends on the assigned covariances used in computing the assimilation cost function. These are discussed in the next section.

5.2. Assigned and estimated observation error variance comparison

In this section, we compare the error variances estimated using the Desroziers *et al.* (2005) diagnostic with those assigned for use in the assimilation cost function (as described in section 4.2). Figure 4 shows the assigned AMV error variance. At high levels, the large assigned variances reflect the poor performance of the model-equivalent observations at these levels. Compared with Figure 2, we see that the assigned error variances are generally larger than those diagnosed. (Note that the axis scales in Figures 2 and 4 are not the same.) Considering the IR108 channel, we see that the diagnosed error variance estimate peaks at the medium level, $14.5 \, m^2 \, s^{-2}$, whereas the assigned error variance peaks at the high level, $66.5 \, m^2 \, s^{-2}$. The effects of the assumed background and observation-error covariances on the diagnosed covariances are complex and competing factors may be at play here. The theoretical study
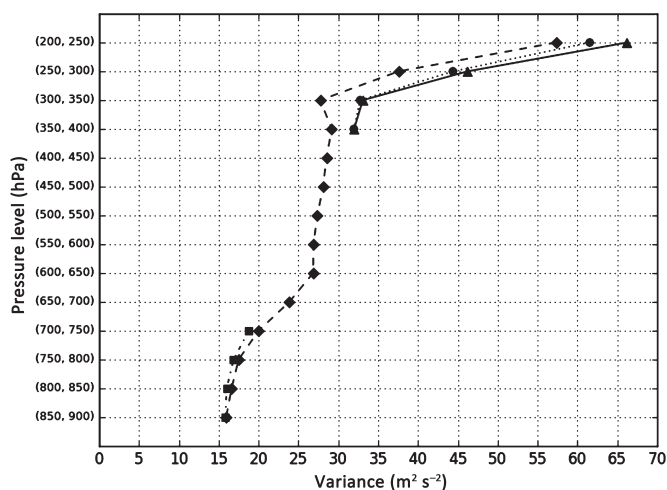

Figure 4. Observation mean assigned error variance $[m^2 \, s^{-2}]$ profile for the four SEVIRI channels: IR108 (dashed with diamonds), WV062 (solid with triangles), WV073 (dotted with circles) and HRVis (dash−dotted with squares). Pressure was discretized in 50 hPa intervals, from 200−900 hPa.
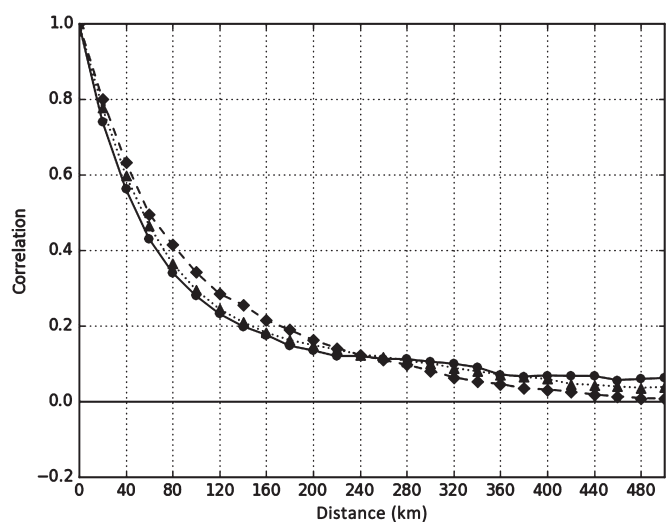

Figure 5. AMV wind-speed observation horizontal error correlation function estimate (20 km bin size) for the three SEVIRI channels, IR108 (solid with circles), WV062 (dashed with diamonds) and WV073 (dotted with triangles), at high level.

by Waller *et al.* (2016b) suggests that, when the assigned observation covariance matrix does not specifically account for correlated errors (as is the case in our experiments) or when the assigned background-error variance is too large, the Desroziers *et al.* (2005) diagnostic tends to underestimate the observation-error variance. On the other hand, assigned observation-error variances that are too large may give diagnosed variances that are overestimated.

5.3. Horizontal observation error correlation estimates

This section shows the results of the AMV horizontal error correlation estimates for the four SEVIRI channels during the JJA 2013 period. The observation-error correlation length-scale is determined when the estimated correlation falls below the threshold value of 0.2 (section 4.3.2).

Figures 5, 6 and 7 show the AMV wind speed (S, Eq. (4)) horizontal error correlation estimates at high level for IR108, WV062 and WV073, medium level for IR108 and low level for IR108 and HRVis, respectively.

Figure 5 shows how the horizontal error correlation function estimates for the three SEVIRI channels IR108, WV062 and WV073 at high level are qualitatively similar. The approximate error correlation length-scales for each channel are found to be $L_{IR108}(\text{high}) \approx 140 \, km$, $L_{WV062}(\text{high}) \approx 180 \, km$
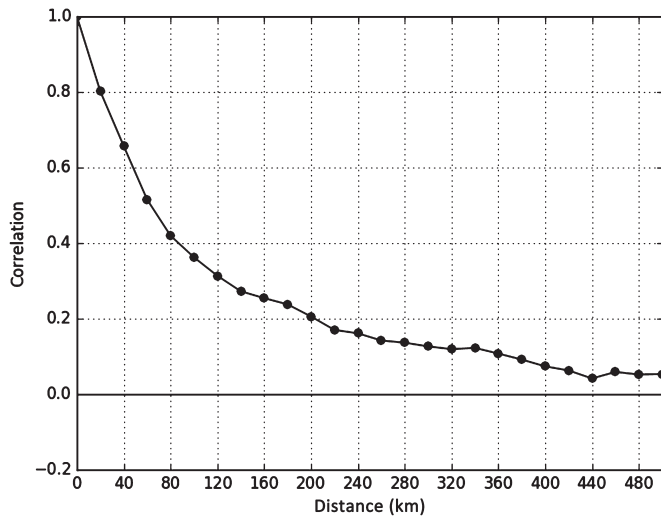
Figure 6. AMV wind-speed observation horizontal error correlation function estimate (20 km bin size) for the SEVIRI channel IR108 (solid with circles) at medium level.
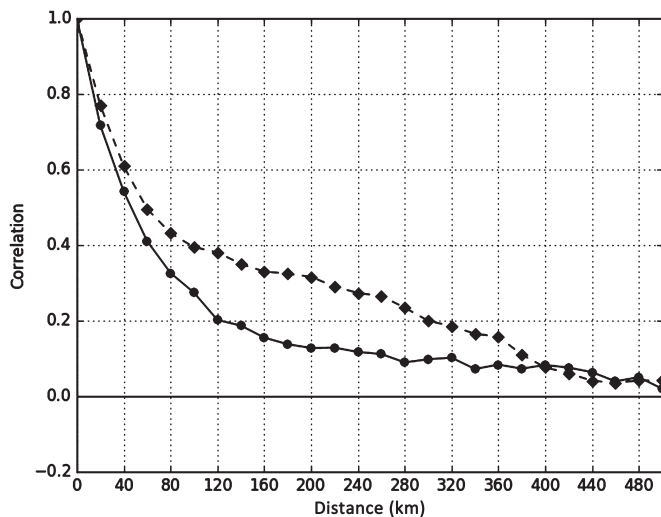

Figure 7. AMV wind-speed observation horizontal error correlation function estimates (20 km bin size) for the two SEVIRI channels IR108 (solid with circles) and HRVis (dashed with diamonds) at the low level.

and $L_{WV073}(high) \approx 140$ km. The spread in the error correlation length-scales at high level can be considered to be relatively small. The similarity in error correlation function estimates could be due to the fact that the AMV derivations for the three SEVIRI channels share the same HRW algorithm, parameters and NWP background. The sources of error correlations at this height seem to be within the same order of magnitude.

Figure 6 shows the estimated horizontal error correlations at mid levels for the IR08 channel. The approximate correlation length-scale is $L_{IR08}(mid) \approx 200$ km. This is somewhat longer than the correlation length-scale at both low and high levels. Compared with Figure 2, we see that the increased estimated correlation length-scale also corresponds to the largest estimated variances.

Figure 7 shows how the horizontal error correlation function estimates for the two SEVIRI channels, IR108 and HRVis, at low level are qualitatively different. The approximate error correlation length-scales are found to be $L_{IR108}(low) \approx 140$ km and $L_{HRVis}(low) \approx 320$ km. In a strict sense, the two SEVIRI channels IR108 and HRVis are not comparable, since HRVis data is not available at night and IR08 data is. These results suggest that at least one source of error has a larger length-scale during daytime than at night-time, $L_{HRVis}(low) > L_{IR108}(low)$. However, the observation-error variance estimate comparison (Table 3) shows that $var(HRViS) < var(IR108)$, suggesting that

Table 4. AMV wind speed (U, V and S components) observation-error horizontal correlation length-scale (km) for the four SEVIRI channels, IR108, WV062, WV073 and HRVis, at high, medium and low levels.

	High level			Medium level			Low level		
	U	V	S	U	V	S	U	V	S
IR108	120	140	140	200	200	200	140	150	140
WV062	160	200	180	–	–	–	–	–	–
WV073	150	170	140	–	–	–	–	–	–
HRVis	–	–	–	–	–	–	320	220	320

the daytime sources of error variance are smaller than the night-time sources of error.

5.4. Length-scale summary

Horizontal observation-error correlations have also been estimated for the two wind-speed vector components, U and V. Table 4 presents the horizontal observation error correlation length-scale for the three wind speed components (U, V and S) for four SEVIRI channels. Results are divided into high, medium and low levels. Table 4 also shows, for the IR channel, how the horizontal observation-error correlation length-scale estimate varies at high, medium and low levels. The largest length-scale is found in the mid levels and is significantly larger than the length-scale for high and low levels. This pattern is similar to the error variance profile, although the exact causes may differ and are not well understood.

As discussed previously, HRVis is not strictly comparable with the other channels, as the AMVs derived from the HRVis channel are only available during the day. Therefore, considering only the three SEVIRI channels, IR108, WV062 and WV073, the wind speed (S component) observation-error correlation length-scale would be within the range $[140–210]$ km. These results are in a good agreement with previous studies ($[120–210]$ km, Table 1).

The horizontal length-scales estimated are significantly larger than the current thinning at the Met Office 3D-Var FGAT high-resolution data assimilation system.

6. Summary

The success of a data assimilation system relies on an accurate specification of the error structures, which weight the relative contribution of the background model and the observations. This work has concentrated on estimating the error structure of atmospheric motion vectors (AMVs), a primary source of wind observations, in a regional-scale model (UK domain) within an operational high-resolution data assimilation system. The new contribution of this work is the use of the Desroziers *et al.* (2005) diagnostic in such a scenario to estimate the AMV error variance vertical profile and horizontal error correlation. The results suggest that the AMV error variance varies significantly over the pressure levels. The largest error variances are found in the mid levels, where wind shear is large and tracked features are more frequently contaminated by features above or below. They may also be a result of high-level winds erroneously being assigned to these mid levels. The overall observation-error variance for the four SEVIRI channels IR108, WV062, WV073 and HRVis considered at high, medium and low levels is estimated to be within $[5.2–14.1]$ m^2 s^{-2} (Table 3). These results are generally a little larger than those derived in previous studies ($[1.5–7.5]$ m^2 s^{-2}, Table 1), although different methodologies and experimental scenarios may have an influence on the exact values. In addition, the results from the Desroziers *et al.* (2005) diagnostic employed are dependent on the assigned error covariance matrices used in the assimilation system (Waller *et al.*, 2016b). Nevertheless, results from the diagnostic still give useful information.

This work has also estimated the horizontal AMV error correlation for the four SEVIRI channels IR108, WV062, WV073 and HRVis considered at high, medium and low levels. For the IR channel, the estimated horizontal error correlation length-scale varies significantly over the pressure levels, with the largest length-scales at medium levels. The results suggest, for the three SEVIRI channels IR108, WV062 and WV073, horizontal error correlation length-scales within the range [140–210] km (Table 4). The HRVis channel results are not strictly comparable with IR108, WV062 and WV073 channels, because the HRVis delivers images during the daytime only. Finally, the horizontal length-scales found are significantly larger than the current thinning used by the Met Office 3D-Var FGAT high-resolution data assimilation system. Since observation errors are dependent on not only the observing instrument but also the observation processing, observation operator and background-field resolution, the observation error statistics estimated in this work are specific to the AMVs and assimilation system used in this study. However, the similarity of our results to those found in previous studies, despite the use of different methodologies and model resolutions, indicates that the errors estimated here may be applicable to different NWP models. This suggests that, in global models with large thinning distances, it may be correct to assume that the observation errors are uncorrelated. However, if AMVs are to be assimilated with thinning distances of order 10 km, then ideally the system would be able to use those correlations in order to specify the observation-error covariance matrix accurately and capitalize on potential improved observation information content, analysis accuracy and forecast skill (Stewart *et al.*, 2008, 2013; Weston *et al.*, 2014; Bormann *et al.*, 2016). However, the diagnosed correlation length-scales are large compared with the limited-area model domain size, so new software strategies are needed in order to incorporate correlated observation errors in this context.

Acknowledgements

References

Ballard SP, Li Z, Simonin D, Caron JF. 2016. Performance of 4D-Var NWP-based nowcasting of precipitation at the Met Office for summer 2012. *Q. J. R. Meteorol. Soc.* **142**: 472–487, doi: 10.1002/qj.2665.

Bedka K, Velden C, Petersen R, Feltz W, Mecikalski J. 2008. Comparison of satellite derived atmospheric motion vectors, radiosonde and NOAA wind profiler observations. *J. Appl. Meteorol. Climatol.* **48**: 1542–1561.

Bormann N, Bauer P. 2010. Estimates of spatial and interchannel observation-error characteristics for current sounder radiances for numerical weather prediction. I: Methods and application to ATOVS data. *Q. J. R. Meteorol. Soc.* **136**: 1036–1050.

Bormann N, Saarinen S, Kelly G, Thepaut J. 2003. The spatial structure of observation errors in atmospheric motion vectors from geostationary satellite data. *Mon. Weather Rev.* **131**: 706–718.

Bormann N, Collard A, Bauer P. 2010a. Estimates of spatial and interchannel observation-error characteristics for current sounder radiances for numerical weather prediction. II: Application to AIRS and IASI data. *Q. J. R. Meteorol. Soc.* **136**: 1051–1063.

Bormann N, Hernandez-Carrascal A, Borde R, Lutz H, Otkin J, Wanzong S. 2010b. Atmospheric motion vectors from model simulations. Part I: Methods and characterization as single-level estimates of wind. *J. Appl. Meteorol. Climatol.* **53**: 147–164.

Bormann N, Hernandez-Carrascal A, Borde R, Lutz HJ, Otkin J, Wanzong S. 2014. Atmospheric motion vectors from model simulations. Part I: Methods and characterization as single-level estimates of wind. *J. Appl. Meteorol. Climatol.* **53**: 47–64.

Bormann N, Bonavita M, Dragani R, Eresmaa R, Matricardi M, McNally A. 2016. Enhancing the impact of IASI observations through an updated observation-error covariance matrix. *Q. J. R. Meteorol. Soc.* **142**: 1767–1780, doi: 10.1002/qj.2774.

Cardinali C. 2009. Monitoring the observation impact on the short-range forecast. *Q. J. R. Meteorol. Soc.* **135**: 239–250.

Chapnik B, Desroziers G, Rabier F, Talagrand O. 2004. Properties and first application of an error-statistics tuning method in variational assimilation. *Q. J. R. Meteorol. Soc.* **130**: 2253–2275.

Chapnik B, Desroziers G, Rabier F, Talagrand O. 2006. Diagnosis and tuning of observational error statistics in a quasi operational data assimilation setting. *Q. J. R. Meteorol. Soc.* **132**: 543–565.

Cotton J, Forsythe M. 2010. 'Fourth analysis of the data displayed on the NWP SAF AMV monitoring website', NWP SAF Technical Report 24. https://nwpsaf.eu/monitoring/amv/analysis.html (accessed 18 October 2016).

Daley R. 1993. Estimating observation-error statistics for atmospheric data assimilation. *Ann. Geophys.* **11**: 634–647.

Desroziers G, Berre L, Chapnik B, Poli P. 2005. Diagnosis of observation, background and analysis-error statistics in observation space. *Q. J. R. Meteorol. Soc.* **131**: 3385–3396.

Desroziers G, Berre L, Chapnik B. 2009. 'Objective validation of data assimilation systems: Diagnosing sub-optimality'. In *Proceedings of ECMWF Workshop on Diagnostics of Data Assimilation System Performance*, 15–17 June 2009. Reading, UK.

Folger K, Weissmann M. 2014. Height corrections of atmospheric motion vectors using satellite LiDAR observations from CALIPSO. *J. Appl. Meteorol. Climatol.* **53**: 1809–1819.

Forsythe M, Doutriaux-Boucher M. 2005. 'Second analysis of the data display on the NWP SAF AMV monitoring website', NWP SAF Technical Report 20. https://nwpsaf.eu/monitoring/amv/nwpsaf_mo_tr_020.pdf (accessed 18 October 2016).

Forsythe M, Saunders R. 2008. 'AMV errors: A new approach in NWP'. In *Proceedings of the 9th EUMETSAT International Winds Workshop*, 14–18 April 2008. Darmstadt, Germany.

García-Pereda J, Marcelino-Rejón M, Fernández-Álvarez P. 2012. 'Algorithm theoretical basis document for high resolution winds', Technical Report SAFNWC/MSG PGE09. http://www.nwcsaf.org (accessed 19 October 2016).

Hernandez-Carrascal A, Bormann N. 2014. Atmospheric motion vectors from model simulations. Part II: Interpretation as spatial and vertical averages of wind and role of clouds. *J. Appl. Meteorol. Climatol.* **53**: 65–82.

Hollingsworth A, Lönnberg P. 1986. The statistical structure of short-range forecast errors as determined from radiosonde data. Part I: The wind field. *Tellus* **38A**: 111–136.

Holmlund K. 1998. The utilization of statistical properties of satellite-derived atmospheric motion vectors to derive quality indicators. *Weather and Forecasting* **13**: 1093–1104.

Joo S, Eyre J, Marriott R. 2012. 'The impact of metop and other satellite data within the Met Office global NWP system using an adjoint-based sensitivity method', *Mon. Wea. Rev.* **141**: 3331–3342, doi: 10.1175/MWR-D-12-00232.1.

Lange H, Janjić T. 2015. Assimilation of Mode-S EHS aircraft observations in COSMO-KENDA. *Mon. Weather Rev.* **144**: 1697–1711, doi: 10.1175/MWR-15-0112.1.

Lean P, Migliorini S, Kelly G. 2015. Understanding atmospheric motion vector vertical representativity using a simulation study and first-guess departure statistics. *J. Appl. Meteorol. Climatol.* **54**: 2479–2500.

Leblanc T, Hauchecorne A. 1997. Recent observations of mesospheric temperature inversions. *J. Geophys. Res.: Atmos.* **102**: 19 471–19 482, doi: 10.1029/97JD01445.

Li H, Kalnay E, Miyoshi T. 2009. Simultaneous estimation of covariance inflation and observation errors within an ensemble Kalman filter. *Q. J. R. Meteorol. Soc.* **128**: 1367–1386.

Liu ZQ, Rabier F. 2002. The interaction between model resolution observation resolution and observation density in data assimilation: A one dimensional study. *Q. J. R. Meteorol. Soc.* **128**: 1367–1386.

Lorenc AC, Rawlins F. 2005. Why does 4D-Var beat 3D-Var? *Q. J. R. Meteorol. Soc.* **131**: 3247–3257.

Lorenc AC, Ballard SP, Bell RS, Ingleby NB, Andrews PLF, Barker DM, Bray JR, Clayton AM, Dalby T, Li D, Payne TJ, Saunders FW. 2000. The Met Office global three-dimensional variational data assimilation scheme. *Q. J. R. Meteorol. Soc.* **126**: 2991–3012.

Mahlman J. 1973. On the maintenance of the polar front jet stream. *J. Atmos. Sci.* **30**: 544–557.

Ménard R. 2016. Error covariance estimation methods based on analysis residuals: Theoretical foundation and convergence properties derived from simplified observation networks. *Q. J. R. Meteorol. Soc.* **142**: 257–273, doi: 10.1002/qj.2650.

Ménard R, Yang Y, Rochon Y. 2009. 'Convergence and stability of estimated error variances derived from assimilation residuals in observation space'. In *Proceedings of ECMWF Workshop on Diagnostics of Data Assimilation System Performance*, 15–17 June 2009. Reading, UK.

Menzel W. 1996. 'Working group 3 report: Verification statistics'. In *Proceedings of the Third International Winds Workshop*, Ascona, Switzerland.

http://cimss.ssec.wisc.edu/iwwg/iww3/index_3rdWindsWorkshop.htm (accessed 18 October 2016).

Miyoshi T, Kalnay E, Li H. 2013. Estimating and including observation-error correlations in data assimilation. *Inverse Prob. Sci. Eng.* **21**: 387–398.

Nieman S, Schmetz J, Menzel W. 1993. A comparison of several techniques to assign heights to cloud tracers. *J. Appl. Meteorol.* **50**: 1559–1568.

Rawlins F, Ballard SP, Bovis KJ, Clayton AM, Li D, Inverarity GW, Lorenc AC, Payne TJ. 2007. The Met Office global four-dimensional variational data assimilation scheme. *Q. J. R. Meteorol. Soc.* **133**: 347–362.

Salonen K, Cotton J, Bormann N, Forsythe M. 2015. Characterizing atmospheric motion vectors height-assignment error by comparing best-fit pressure statistics from the Met Office and ECMWF data assimilation systems. *J. Appl. Meteorol. Climatol.* **54**: 544–557.

Schmetz J, Holmlund K, Hoffman J, Strauss B. 1993. Operational cloud-motion winds from Meteosat infrared images. *J. Appl. Meteorol.* **32**: 1206–1225.

Schmetz J, Pili P, Tjemkes S, Just D, Kerkmann J, Rota S, Ratier A. 2002. An introduction to Meteosat Second Generation (MSG). *Bull. Am. Meteorol. Soc.* **83**: 977–992.

Schmid J. 2000. 'The SEVIRI instrument'. In *Proceedings of the 2000 EUMETSAT Meteorological Satellite Data User's Conference*, 29 May–2 June 2000, Bologna, Italy.

Schraff C, Reich H, Rhodin A, Schomburg A, Stephan K, Periáñez A, Potthast R. 2016. Kilometre-scale ensemble data assimilation for the COSMO model (Kenda). *Q. J. R. Meteorol. Soc.* **142**: 1453–1472, doi: 10.1002/qj.2748.

Stewart LM. 2010. 'Correlated observation errors in data assimilation', PhD thesis. University of Reading: Reading, UK. http://www.reading.ac.uk/maths-and-stats/research/theses/maths-phdtheses.aspx (accessed 18 October 2016).

Stewart L, Dance S, Nichols N. 2008. Correlated observation errors in data assimilation. *Int. J. Numer. Methods Fluids* **56**: 1521–1527.

Stewart LM, Cameron J, Dance SL, English S, Eyre JR, Nichols NK. 2009. 'Observation error correlations in IASI radiance data', Technical Report number 1/2009. Mathematics reports series. University of Reading. www.reading.ac.uk/web/FILES/maths/obs_error_IASI_radiance.pdf (accessed 18 October 2016).

Stewart L, Dance S, Nichols N. 2013. Data assimilation with correlated observation errors: Experiments with a 1-D shallow water model. *Tellus A* **65**: 1–14.

Stewart LM, Dance SL, Nichols NK, Eyre JR, Cameron J. 2014. Estimating interchannel observation-error correlations for IASI radiance data in the Met Office system. *Q. J. R. Meteorol. Soc.* **140**: 1236–1244, doi: 10.1002/qj.2211.

Todling R. 2015. A complementary note to A lag-1 smoother approach to system-error estimation: The intrinsic limitations of residual diagnostics. *Q. J. R. Meteorol. Soc.* **141**: 2917–2922, doi: 10.1002/qj.2546.

Velden C, Bedka K. 2009. Identifying the uncertainty in determining satellite-derived Atmospheric Motion Vectors vector height attribution. *J. Appl. Meteorol. Climatol.* **48**: 450–463.

Waller JA, Dance SL, Lawless AS, Nichols NK. 2014a. Estimating correlated observation-error statistics using an ensemble transform Kalman filter. *Tellus A* **66**: 23294. doi: 10.3402/tellusa.v66.23294.

Waller JA, Dance SL, Lawless AS, Nichols NK, Eyre JR. 2014b. Representativity error for temperature and humidity using the Met Office high-resolution model. *Q. J. R. Meteorol. Soc.* **140**: 1189–1197, doi: 10.1002/qj.2207.

Waller JA, Ballard SP, Dance SL, Kelly G, Nichols NK, Simonin D. 2016a. Diagnosing horizontal and inter-channel observation-error correlations for SEVIRI observations using observation-minus-background and observation-minus-analysis statistics. *Remote Sens.* **8**: 581, doi: 10.3390/rs8070581.

Waller JA, Dance SL, Nichols NK. 2016b. Theoretical insight into diagnosing observation-error correlations using observation-minus-background and observation-minus-analysis statistics. *Q. J. R. Meteorol. Soc.* **142**: 418–431, doi: 10.1002/qj.2661.

Waller JA, Simonin D, Dance SL, Nichols NK, Ballard SP. 2016c. Diagnosing observation-error correlations for Doppler radar radial winds in the Met Office UKV model using observation-minus-background and observation-minus-analysis statistics. *Mon. Weather Rev.* **144**: 3533–3551, doi: 10.1175/MWR-D-15-0340.1.

Weston PP, Bell W, Eyre JR. 2014. Accounting for correlated error in the assimilation of high-resolution sounder data. *Q. J. R. Meteorol. Soc.* **140**: 2420–2429, doi: 10.1002/qj.2306.